PHYSICAL REVIEW A **86**, 023421 (2012)

Tracking molecular wave packets in cesium dimers by coherent Raman scattering

Luqi Yuan,[1] Dmitry Pestov,[2] Robert K. Murawski,[3] Gombojav O. Ariunbold,[4,5] Miaochan Zhi,[1] Xi Wang,[1] Vladimir A. Sautenkov,[1,6] Yuri V. Rostovtsev,[7] Torsten Siebert,[1,8] and Alexei V. Sokolov[1]

[1]*Texas A&M University, College Station, Texas 77843, USA*
[2]*Biophotonic Solutions Inc., 1401 East Lansing Drive, Suite 112, East Lansing, Michigan 48823, USA*
[3]*Department of Physics, Drew University, Madison, New Jersey 07940, USA*
[4]*The University of Arizona, College of Optical Sciences, Tucson, Arizona 85721, USA*
[5]*School of Physics and Electronics, National University of Mongolia, Ulaanbatar 210646, Mongolia*
[6]*Joint Institute for High Temperatures of Russian Academy of Sciences, 13-2 Izhorskaya Str., Moscow 125412, Russia*
[7]*Department of Physics, University of North Texas, Denton, Texas 76203, USA*
[8]*Institut für Experimentalphysik, Freie Universität Berlin, Arnimallee 14, 14195 Berlin, Germany*

(Received 5 April 2012; published 31 August 2012)

We explore wave-packet dynamics in the ground $X\ ^1\Sigma_g^+$ and excited $B\ ^1\Pi_u$ states of cesium dimers (Cs_2). In particular, we study the dependence of the wave-packet dynamics on the relative timing between femtosecond pump, Stokes, and probe pulses in a nondegenerate BOXCARS beam geometry, which are commonly used for coherent anti-Stokes Raman scattering (CARS) spectroscopy. The experimental results are elucidated by theoretical calculations, which are based on the Liouville equations for the density matrix for the molecular states. We observe oscillations in CARS signals as functions of both Stokes and probe pulse delays with respect to the pump pulse. The oscillation period relates to the wave-packet motion cycle in either the ground or excited state of Cs_2 molecules, depending on the sequence of the input laser pulses in time. The performed analysis can be applied to study and/or manipulate wave-packet dynamics in a variety of molecules. It also provides an excellent test platform for theoretical models of molecular systems.

DOI: 10.1103/PhysRevA.86.023421 PACS number(s): 33.80.−b, 33.80.Wz, 78.47.nj, 42.65.Re

I. INTRODUCTION

Femtosecond laser pulses have been used to study the transient ultrafast dynamical processes in molecular systems and launched a research field, which is called femtochemistry [1,2]. The study of the vibrational and rotational wave packets in molecules on femtosecond time scale has been of interest for several decades [3]. Recently, the vibrational and rotational wave-packet dynamics in different molecules have been observed by adopting the two-color, pump probe [4–6] and coherent femtosecond four-wave mixing (FWM) spectroscopic [7–10] techniques. Resonant coherent anti-Stokes Raman scattering (CARS) spectroscopy has been used to extract a time-dependent wave function of a reacting molecule [11]. It has been shown that the phase-matching condition in the FWM process is crucial in monitoring the molecular dynamics at single-laser-shot level [12,13]. The effect of the impulsive excitation and the momentum transfer [14,15] exists in the FWM experiment with ultrashort pulses.

Coherent laser control of the quantum dynamics in the physicochemical processes has been studied [2,16]. In particular, temporal coherent control on ultrashort time scale in atomic rubidium vapor has been reported [17,18]. The study of quantum interference of molecular eigenstates has led to a method to manipulate the wave packets with promising applications in various coherent control techniques [19]. Two-dimensional spectroscopy has served as a useful tool, which provides a clear physical picture of the wave-packet temporal evolution [20]. Coherent optical response in gas has been revealed by using the Fourier transform of two-dimensional spectroscopic measurements [21,22]. A time-dependent perturbation theory has been adopted to understand various FWM processes [23–25]. Density matrix formalism [26] has proved to be an important tool to interpret molecular coherent processes observed in femtosecond experiments [27,28].

In the present work, we study ultrafast wave-packet dynamics in cesium dimers by using the CARS technique in the nondegenerate BOXCARS beam arrangement. The main advantage of our experimental configuration is the ability to perform two-dimensional types of measurements. In particular, the measured CARS signal is studied as a two-dimensional function of pump-Stokes and pump-probe delays. In order to model these experiments, we adopt the Liouville's equation for the density matrix for the electronic excited ($B\ ^1\Pi_u$) and ground ($X\ ^1\Sigma_g^+$) states with the appropriate Franck-Condon factors. The electric dipole moment between the ($B\ ^1\Pi_u$) and ($X\ ^1\Sigma_g^+$) states could be approximated to be a constant if the locations of the nuclei are not displaced far from the equilibrium [29]. In our experiment, we note that the rotational levels are also heavily populated. However, for simplicity's sake, the rotational contributions have been neglected in the theoretical model with the Franck-Condon principle.

Our paper is organized as follows. We present the experimental setup and theoretical model in the next two sections. In Sec. IV, the experimental and theoretical results are analyzed in detail. We summarize our results in the last section.

II. EXPERIMENTAL SETUP

The Cs_2 wave-packet dynamics is studied via a two-color CARS scheme. The input pump, Stokes, and probe beams are arranged in the folded-BOXCARS geometry. The experimental setup is shown in Fig. 1.

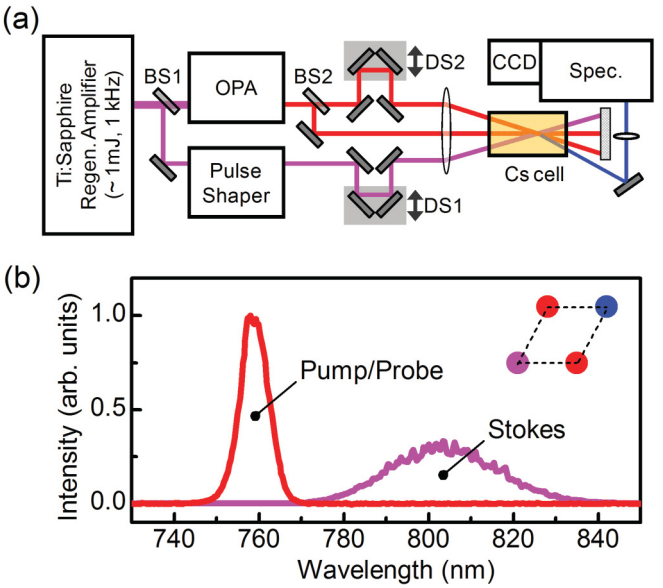

FIG. 1. (Color online) An experimental setup: (a) A schematic layout. OPA, optical parametric amplifier; BS1,2, beamsplitter; DS1,2, delay stage; Spec., spectrograph; CCD, charge coupled device. (b) The measured spectra of pump, probe, and Stokes beams. Inset: A folded-BOXCARS beam arrangement used in the experiment. A spot on the top right corner (blue) corresponds to the phase-matched CARS signal and the other spots correspond to the input beams.

We use a commercially available femtosecond Ti:sapphire regenerative amplifier system (Legend, Coherent) and an optical parametric amplifier (OPA: OPerA-VIS/UV, Coherent) to generate passively synchronized 1-kHz pulse trains of the two colors. The pump and probe beams are produced by splitting the output beam of the OPA and tuned to center wavelength 760 nm [see Fig. 1(b)]. The spectral full-width-at-half-maximum (FWHM) is about 12 nm. For the pump and probe beams, average power is attenuated to about 1 mW (corresponds to 1 μJ/pulse) in front of the Cs cell. For the Stokes beam, we use a small fraction of the regenerative amplifier output beam. Its spectrum is centered at 805 nm, and the spectral FWHM is close to 30 nm. The beam passes through a pulse shaper (Silhouette, Coherent), which corrects phase distortions along the Stokes beam path down to the Cs cell by means of multiphoton intrapulse interference phase scan (MIIPS) [30]. The Stokes pulse energy at the target is $\sim$0.1 μJ. The relative timing between the pump, Stokes, and probe pulses is adjusted by the two automated delay lines. All the beams are focused and overlapped (under $\sim 2 \times 10^{-2}$ rad angle) inside a 7.5-cm long Cs cell heated up to 240 °C. At this temperature, the number density of Cs_2 molecules is about 2.3×10^{13} cm^{-3} [31]. However we note that the number density of cesium atoms is approximately two orders of magnitude higher than that for Cs_2 molecules.

The generated CARS signal (near 720 nm) is spatially filtered and focused by a lens at the entrance slit of a spectrograph (Chromex Spectrograph 250is) with a liquid-nitrogen-cooled CCD (Spec-10, Princeton Instruments). For most of our measurements, the detected signal is spectrally integrated over a narrow band, filtering the residual pump and probe contributions.

III. THEORETICAL MODEL

In this section, we present a theoretical model suitable to interpret the time-delayed coherent Raman scattering measurement. We classify the present problem by the order of the arrival times of the three input pulses into the cell. First we consider the case of Stokes-pump-probe configuration where the Stokes pulse arrives first followed by the pump and probe pulses. In this case, there are two possible pathways as shown in Fig. 2. The upper levels, $|a\rangle$ and $|a'\rangle$, are the vibrational levels in the excited state, $B\ ^1\Pi_u$, while the lower two, $|b\rangle$ and $|c\rangle$, are the vibrational levels in the ground state, $X\ ^1\Sigma_g^+$. Note that the level here represents many closely spaced energy levels. The initial population is equally distributed over all the vibrational levels in the ground state. A reason is that the cesium dimer is produced by the hot cesium atomic collisions, which excites the cesium molecules to the upper vibrational levels in the ground state. A nonradiative relaxation between vibrational levels enables the molecules being equally populated over all the ground-state vibrational levels.

The derivations of the equations that describe the both pathways are similar. In particular, for pathway (a) in Fig. 2, the Hamiltonian under the near-resonance approximation is

$$H = H_0 + H_I, \tag{1}$$

where the unperturbed part of the Hamiltonian is

$$H_0 = \hbar\omega_{a'}|a'\rangle\langle a'| + \hbar\omega_a|a\rangle\langle a| + \hbar\omega_b|b\rangle\langle b| + \hbar\omega_c|c\rangle\langle c|, \tag{2}$$

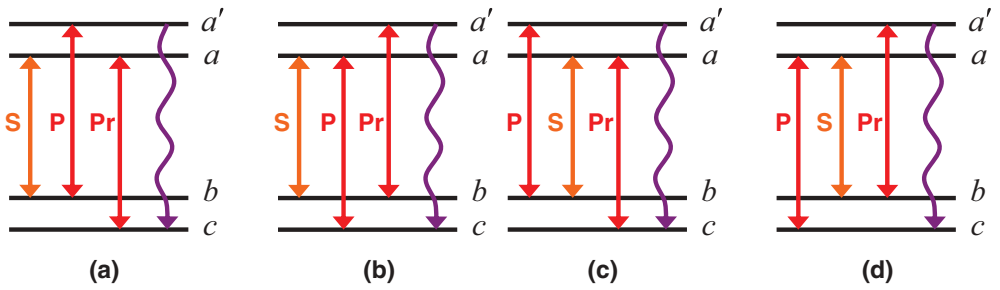

FIG. 2. (Color online) Energy level diagrams for the two possible pathways [(a) and (b)] in the Stokes-pump-probe configuration and the other two possible pathways [(c) and (d)] in the pump-Stokes-probe configuration. The upper (lower) two levels are the vibrational levels in the excited (ground) electronic state.

and the interaction part of the Hamiltonian is

$$H_I = -\wp_{ab}E_s|a\rangle\langle b| - \wp_{a'b}E_p|a'\rangle\langle b| - \wp_{ac}E_{pr}|a\rangle\langle c| + \text{H.c.}. \tag{3}$$

The energy $\hbar\omega$ for the vibrational level v is defined as [32]

$$\hbar\omega = \hbar\omega_e\left(v+\tfrac{1}{2}\right) - \hbar\omega_e\chi_e\left(v+\tfrac{1}{2}\right)^2, \tag{4}$$

where ω_e is the vibrational frequency of the corresponding electronic state and $\omega_e\chi_e$ is the vibrational anharmonicity. The pulse field is described by a Gaussian shape pulse as

$$E_i = \mathcal{E}_i \exp\left[-\frac{1}{2}\left(\frac{t-\tau_i}{\sigma_i}\right)^2\right]\cos\left[\nu_i\,(t-\tau_i) - \mathbf{k}_i\cdot\mathbf{x}\right], \tag{5}$$

where i stands for s, p, and pr representing Stokes, pump, and probe, respectively, τ_i is the time delay of the pulse, σ_i is the spectral width, ν_i is the frequency of the pulse, and $\mathbf{k}_i$ is the wave vector. The equation of motion for the density matrix is [26]

$$\dot{\rho} = -\frac{i}{\hbar}[H,\rho]. \tag{6}$$

There are no relaxation terms in this equation because the effective lifetime of the cesium molecule due to the frequent collisions with the cesium atoms (about 1 ns) is much longer than the time scale (∼1 ps) considered in the present experiment. The signal intensity is given by

$$S = \int_{-\infty}^{\infty}\left|\sum \wp_{ca'}\rho_{a'c} + \text{c.c.}\right|^2 dt. \tag{7}$$

The initial conditions here are $\rho_{ij}(-\infty) = 0$, except for that $\rho_{bb}(-\infty) = \rho_{bb}^{(-\infty)}$ and $\rho_{cc}(-\infty) = \rho_{cc}^{(-\infty)}$.

If three pulses do not coincide in time, we can find a general solution for the signal under the first-order approximation and rotating-wave approximation (RWA) (see Appendix A),

$$\begin{aligned} S \simeq \sum_{a'}\sum_{a,a_1}\sum_{b,b_1}\sum_{c}\left(\frac{\pi}{2}\right)^3\frac{1}{\gamma}|\rho_{bb}^{(-\infty)}|^2\wp_{ca'}\wp_{a'b}\wp_{ba}\wp_{ac}\wp_{a'c}\wp_{b_1a'}\wp_{a_1b_1}\wp_{ca_1}(\mathcal{E}_s\mathcal{E}_p\mathcal{E}_{pr}\sigma_s\sigma_p\sigma_{pr})^2 \\ \times\exp\left\{-\frac{1}{2}[\sigma_s(\nu_s-\omega_{ab})]^2 - \frac{1}{2}[\sigma_p(\nu_p-\omega_{a'b})]^2 - \frac{1}{2}[\sigma_{pr}(\nu_{pr}-\omega_{ac})]^2\right\} \\ \times\exp\left\{-\frac{1}{2}[\sigma_s(\nu_s-\omega_{a_1b_1})]^2 - \frac{1}{2}[\sigma_p(\nu_p-\omega_{a'b_1})]^2 - \frac{1}{2}[\sigma_{pr}(\nu_{pr}-\omega_{a_1c})]^2\right\} \\ \times\cos[\omega_{aa_1}(\tau_{pr}-\tau_s) - \omega_{bb_1}(\tau_p-\tau_s)]. \end{aligned} \tag{8}$$

Eq. (8) shows the generated field intensity for the Stokes-pump-probe configuration associated with the first pathway in Fig. 2(a). Later, we will use this result explicitly in the simulation.

Next we introduce the Franck-Condon factors. The electric dipole transition moment, $\wp_{v'v''}$, between the vibrational level v' in the excited electronic state and the vibrational level v'' in the ground electronic state is shown as [29]

$$\wp_{v'v''} = \mu S(v',v''), \tag{9}$$

where μ is the electronic transition moment, which is a constant when the displacement of the nuclei from their equilibrium is relatively small, and $S(v',v'') = \int \psi_{v'}^*(R)\psi_{v''}(R)d\tau_N$, is the overlap integral between two vibrational eigenstates.

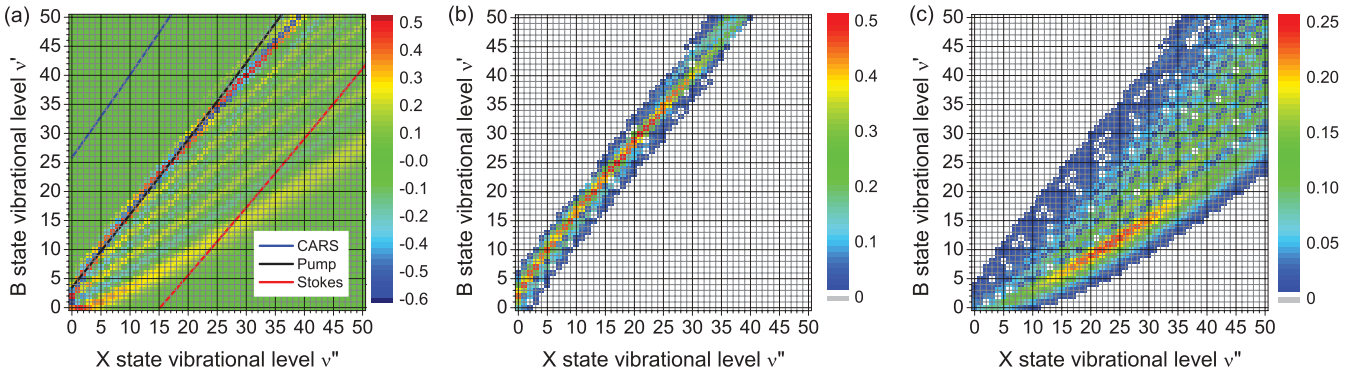

FIG. 3. (Color online) (a) The overlap integral, $S(v',v'')$ between the vibrational levels in the ground state $X\,^1\Sigma_g^+$, and excited state $B\,^1\Pi_u$. The darker of the red (blue) color the larger is the positive (negative) number. The black, red, and blue lines show the center wavelengths of the pump or probe, Stokes, and signal, respectively. The product of $|S(v',v'')|$ and the Gaussian beam profile show the transition efficiencies for the pump or probe field (b) and Stokes field (c).

Here R is the internuclear distance and τ_N is the volume element in terms of the nuclear coordinates [33]. The square of this integral is the well-known Franck-Condon factor. Figure 3(a) shows the calculated overlap integral, $S(\nu',\nu'')$, between the vibrational levels in the ground and excited states. Figures 3(b) and 3(c) show the product of $|S(\nu',\nu'')|$ and Gaussian beam profile $\exp[-\frac{1}{2}(\frac{t-\tau_i}{\sigma_i})^2]$ for the pump or probe field and the Stokes field respectively. The pump or probe wavelength is strongly resonant to a number of transitions. At this point the Stokes wavelength plays an important role for the specific selection of the underlining processes. It couples primarily the 13–33 vibrational levels in the X state and 5–17 vibrational levels in the B state. For the FWM process we should also notice that the 2–10 vibrational levels in the X state is coupled to the 5–17 vibrational levels in the B state whereas the 20–43 vibrational levels in the B state is coupled to the 13–33 vibrational levels in the X state strongly by the pump or probe beam. The signal wavelength is not favored by the Franck-Condon factors, so it is only weakly coupled to any resonant transition. Later we will discuss these transitions based on the simulations, which include the Franck-Condon factors.

By considering the effect of the Franck-Condon factor in detail as shown in Appendix B, we can simplify Eq. (8) as

$$S \propto \sum_{a',a,b,c} |\wp_{ca'}\wp_{a'b}\wp_{ba}\wp_{ac}|^2\{1+\cos[\omega_{b+1,b}(\tau_p-\tau_s)+\pi] + \cos[\omega_{a+1,a}(\tau_{pr}-\tau_s)+\pi]+\cos[\omega_{a+1,a}(\tau_{pr}-\tau_s) - \omega_{b+1,b}(\tau_p-\tau_s)]\}. \quad (10)$$

This simplified result of the signal intensity in the first pathway in Fig. 2(a) will be used later to explain the results of the experimental measurements.

Following the similar procedure, for the second pathway [Fig. 2(b)], we can find the signal as

$$S \simeq \sum_{a'}\sum_{a,a_1}\sum_{b,b_1}\sum_{c}\left(\frac{\pi}{2}\right)^3\frac{1}{\gamma}\left|\rho_{bb}^{(-\infty)}\right|^2\wp_{ca'}\wp_{a'b}\wp_{ba}\wp_{ac}\wp_{a'c}\wp_{b_1a'}\wp_{a_1b_1}\wp_{ca_1}(\mathcal{E}_s\mathcal{E}_p\mathcal{E}_{pr}\sigma_s\sigma_p\sigma_{pr})^2 \times \exp\left\{-\frac{1}{2}[\sigma_s(\nu_s-\omega_{ab})]^2-\frac{1}{2}[\sigma_p(\nu_p-\omega_{ac})]^2-\frac{1}{2}[\sigma_{pr}(\nu_{pr}-\omega_{a'b})]^2\right\} \times \exp\left\{-\frac{1}{2}[\sigma_s(\nu_s-\omega_{a_1b_1})]^2-\frac{1}{2}[\sigma_p(\nu_p-\omega_{a_1c})]^2-\frac{1}{2}[\sigma_{pr}(\nu_{pr}-\omega_{a'b_1})]^2\right\} \times \cos[\omega_{bb_1}(\tau_{pr}-\tau_s)-\omega_{aa_1}(\tau_p-\tau_s)], \quad (11)$$

and the corresponding simplified equation reads

$$S \propto \sum_{a',a,b,c} |\wp_{ca'}\wp_{a'b}\wp_{ba}\wp_{ac}|^2\{1+\cos[\omega_{a+1,a}(\tau_p-\tau_s)+\pi] + \cos[\omega_{b+1,b}(\tau_{pr}-\tau_s)+\pi] + \cos[\omega_{b+1,b}(\tau_{pr}-\tau_s)-\omega_{a+1,a}(\tau_p-\tau_s)]\} \quad (12)$$

Similar derivations are also used to find the signals for two possible pathways in Figs. 2(c) and 2(d) in the pump-Stokes-probe pulse sequence.

IV. RESULTS AND DISCUSSION

In this section we give interpretations for the observed experimental data based on the results obtained from the theoretical model presented in the previous section. The parameters for the cesium molecule used to calculate the corresponding vibrational frequency in Eq. (4) are taken from Ref. [5], namely $\omega_e = 42.02\ \text{cm}^{-1}$ and $\omega_e\chi_e = 0.0819\ \text{cm}^{-1}$ for the ground electronic state, $X\,^1\Sigma_g^+$, while $\omega_e = 34.33\ \text{cm}^{-1}$ and $\omega_e\chi_e = 0.0800\ \text{cm}^{-1}$ for the excited electronic state, $B\,^1\Pi_u$.

In Fig. 4, we present the experimental results in the Stokes-pump-probe pulse sequence [Fig. 4(a)]. The Stokes pulse arrives at time zero followed by the pump pulse after a fixed delay at about 1.5 times the wave packet oscillating period (0.86 ps) in the ground state, which is 1.5×0.86 ps. The FWM signal is shown in Fig. 4(b). After integrating over the spectral positions from the data in Fig. 4(b), the oscillating dependence on the probe delay is clearly illustrated in Fig. 4(d). The corresponding fast Fourier transform (FFT) spectra is given in the insets [see Figs. 4(c) and 4(d)]. It exhibits an oscillation dominated by the frequency 29.3 cm^{-1}, which is approximately the vibrational frequency in the excited electronic state. One should notice that there are also negative values of the probe pulse delays in both Figs. 4(b) and 4(d). This corresponds to the case that the probe pulse arrives before the pump pulse.

Simplified equations Eq. (10) and Eq. (12) for the signal intensity under the conditions of the two possible pathways in the Stokes-pump-probe pulse sequence enable us to interpret the experimental results. First of all, let us carefully examine Eq. (10) for the first pathway as in Fig. 2(a). The second term, $\cos[\omega_{b+1,b}(\tau_p-\tau_s)+\pi]$, includes the vibrational frequency of the upper vibrational levels in the ground state, $\omega_{b+1,b}$, and the time delay between the pump pulse and the Stokes pulse. This is the same "laser control" term as discussed in Ref. [16]. This term controls the amplitude of the signal intensity depending on the time delays between the first two pulses. Moreover, there is an extra "π" phase as a result of the overlap integrals between different vibrational eigenstates. This phase plays an important role, which results in the strongest signal when the first two pulses' time delays are $0.5T_g$, $1.5T_g$, $2.5T_g$, and so forth. (Here, T_g is the cycling period of the wave packet in the ground vibrational states.)

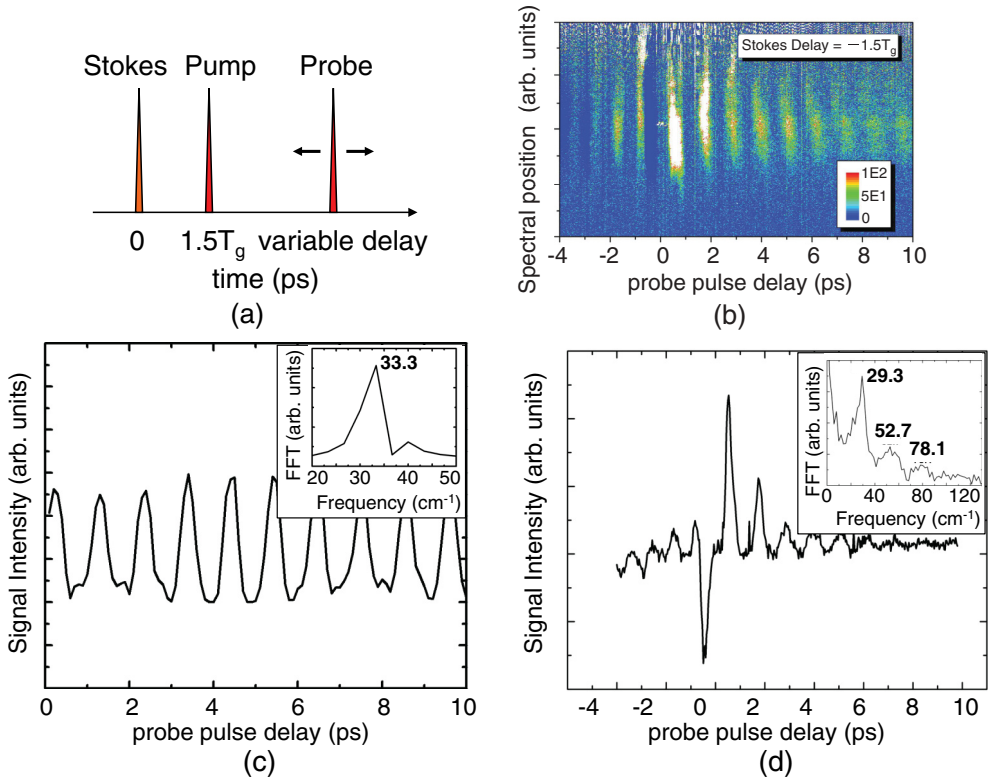

FIG. 4. (Color online) (a) Stokes-pump-probe pulse sequence. (b) The experimental data for the spectrum of the FWM signal as a function of probe delay. (c) The theoretical results for the signal versus probe delay. (d) The integrated spectrum from the experimental data in (b). The insets in (c) and (d) show the corresponding FFT spectra.

More explicitly the occurrence of the extra π phase is a result of the resonant conditions. In particular, the pump pulse at 760 nm is resonant to the left-hand side (for the shorter internuclear distance), while the Stokes pulse at 800 nm is resonant to the right-hand side (for the longer internuclear distance) of the potential curves (see Fig. 5).

The third term, $\cos[\omega_{a+1,a}(\tau_{pr} - \tau_s) + \pi]$, consists of the vibrational frequency in the excited state, and the time delay between the probe pulse and the Stokes pulse. Therefore, this term contributes to the signal oscillation with respect to the probe pulse delay.

Similarly, Eq. (12) for the second pathway as in Fig. 2(b) shows another laser control term, $\cos[\omega_{a+1,a}(\tau_p - \tau_s) + \pi]$. This time, it depends on the period defined by the vibrational level spacing in the excited state. The next term, $\cos[\omega_{b+1,b}(\tau_{pr} - \tau_s) + \pi]$ is related to the vibrational frequency in the ground state and determines the oscillation with respect to the probe pulse delay.

Therefore, the timing of the pump and Stokes pulses determine the combined contribution of the two pathways in the overall process. Especially, one of the two pathways could dominate over the other one. In the present experiment with the particular pulse sequence as Fig. 4(a), the time delay between the first two pulses is one and one half of the ground state period (1.5 × 0.86 ps). This means that the first pathway dominates over the second one. The signal intensity mainly oscillates at a vibrational frequency of the excited state, which is consistent with the experimental observation [Fig. 4(d)].

To further clarify the physics insight of this process [see, Fig. 2(a)] for the pulse sequence given in Fig. 4 (a), we demonstrate temporal evolution (within interval from zero to $1.5T_g$) of the wave packet in Fig. 5. The Stokes pulse arrives at time zero and generates the wave packet in the ground state, $X\ ^1\Sigma_g^+$, and the wave packet in the excited state, $B\ ^1\Pi_u$. Both wave packets initially focus on the right side (with respect to the minimum position of the potential energy curves) where the Stokes pulse is resonant to the potential energy difference. As time passes by, these two wave packets start to move back and forth, with different cycling periods according to the different vibrational frequencies in the ground and excited states. The pump pulse arrives at $1.5T_g$ and is resonant to the left side of the difference between interaction potentials. Thus, the pump field can either pump the population up again [see the first pathway in Fig. 2(a)], or "dump" the population down [see the second pathway in Fig. 2(b)]. However at this particular time, the wave packet in the excited state is spread out but the wave packet in the ground state is localized to the left side. Therefore, the first pathway is the dominant process in this case.

So far, we have shown how simple results, Eqs. (10) and (12) can easily interpret our experimental results. We also perform numerical simulations to solve the general equations (8) and (11). Figure 4(c) shows the numerical results of the signal intensity versus the probe pulse delay for the pulse sequence as shown in Fig. 4(a). The numerical result agrees well with the experimental result in Fig. 4(d). It shows that the oscillation of

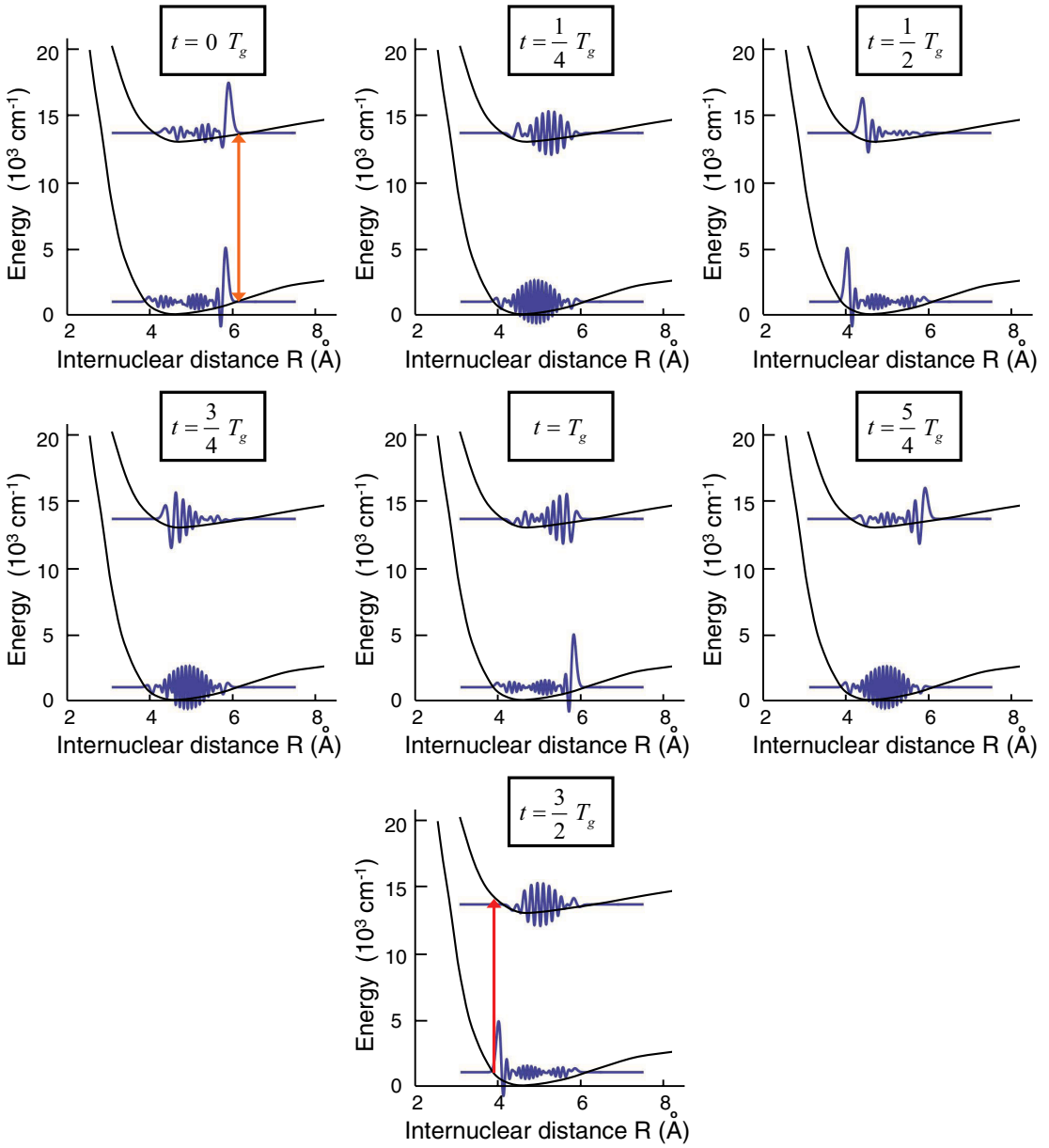

FIG. 5. (Color online) Temporal evolution of the wave packets created in the excited and ground states in Cs_2 molecules. The Stokes pulse arrives at time zero and the pump pulse arrives later at $1.5T_g$ for pulse sequence given in Fig. 4(a).

the signal intensity has the same frequency with the vibrational frequency in the excited state.

Next we consider the case of the pump-Stokes-probe configuration as in Fig. 6(a). The Stokes pulse is delayed at a fixed value ($1.5T_g$) and the probe delay is varied with respect to the pump arrival time. The experimental results are shown in Figs. 6(b) and 6(d), where the signal exhibits the oscillation with a frequency ($\sim$29.3 cm^{-1}) associated with the excited state. Analogous analysis as for the Stokes-pump-probe configuration can be done in this case to elucidate the observed data. Similarly, there are two possible pathways as shown in Figs. 2(c) and 2(d). For the pathway in Fig. 2(c), the time delay between the first two pulses is a laser control parameter, together with the ground-state vibrational frequency. However, the oscillation frequency is determined by the time delay between the probe and pump pulses together with the excited state vibrational frequency. Theoretical (numerical) simulation shows the signal oscillation with the excited-state vibrational frequency [see Fig. 6(c)].

Moreover, we also measured the FWM signal where the pump and probe pulses overlap in time and the Stokes pulse is delayed. Figure 7 shows the experimental measurement and the energy level diagram for Cs atoms. The experimental results exhibit an oscillating signal with the frequency of 21 cm^{-1}. The two-photon process for the pump and probe beams is resonant with the transition between 6*s* and 7*d* levels in Cs atoms. Thus, coherence between these two levels is prepared. A delayed Stokes field then triggers the generation of the FWM signal in the Cs atoms. This FWM signal is relatively strong compared to that for Cs_2 molecules as we mentioned earlier that there

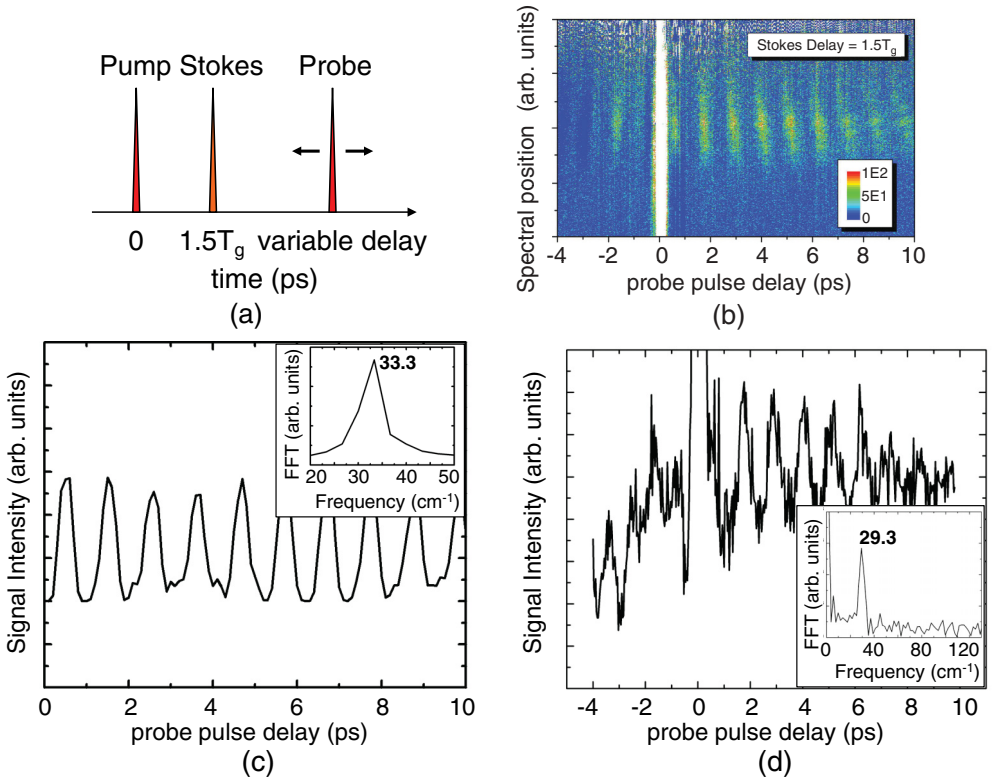

FIG. 6. (Color online) (a) Pump-Stokes-probe pulse sequence. (b) The experimental data for the spectrum of the FWM signal as a function of probe delay. (c) The theoretical results for the signal versus probe delay. (d) The integrated spectrum from the experimental data in (b). The insets in (c) and (d) show the corresponding FFT spectra.

are much more Cs atoms rather than Cs_2 molecules in the cell. We notice that the degeneracy of the $7d$ level in Cs atoms and the energy difference between levels $7d\ ^2D_{5/2}$ and $7d\ ^2D_{3/2}$ is 20.92 cm^{-1}. The FWM signal is a result of the beating at frequency of 20.92 cm^{-1} due to the splitting of $7d$ energy level.

Let us consider the FWM signal in Cs_2 molecules when the pump and probe pulses are not overlapped. A two-dimensional measurement result is shown in Fig. 8(a). The measurement is performed when varying delays of both the Stokes and probe pulses separately. The measurement exhibits a periodic pattern.

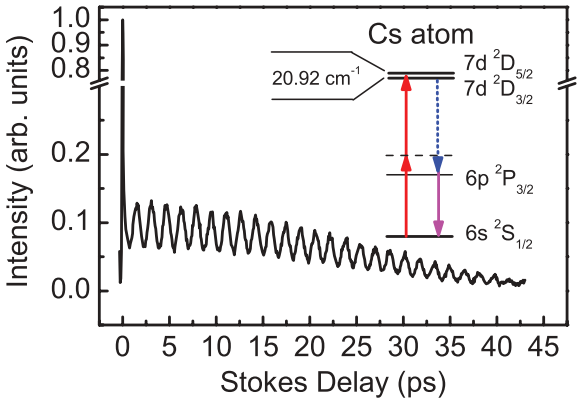

FIG. 7. (Color online) Experimental measurement where the pump and probe beams are overlapped in time and the Stokes pulse is delayed. Inset: energy level diagram for Cs atoms.

It reveals the complex wave-packet motions interacting with the laser pulses via all the possible pathways in Cs_2 molecules. The dark red area in the middle of the measured pattern corresponds to the overlap of the pump and probe pulses. In this area, two-photon absorption process in the Cs atom results in a strong FWM signal as we discussed above. The simulation based on the above mentioned theory [Eqs. (8) and (11) for the Stokes-pump-probe pulse sequence and analogous equations for the pump-Stokes-probe pulse sequence] in the Cs_2 molecule is performed [see Fig. 8(b)]. Note that in the simulation, the two-photon absorption process for the Cs atom is not included. Such two-photon absorption process occurs when the pump and probe pulses are overlapped (i.e., $\tau_p = \tau_{pr}$) as discussed in the previous paragraph and for the pump-probe-Stokes sequence (i.e., $\tau_p < \tau_{pr} < \tau_s$). (In the latter case, the delayed probe pulse is overlapped with the pump pulse's weak oscillating tail, which is created by the modulation between the pump pulse and the Cs_2 molecule.) The periodic pattern is also obtained in the theoretical two-dimensional plot. It shows the interaction between the laser pulses and the Cs_2 molecules under all the possible pathways. As seen from Figs. 8(a) and 8(b), the theoretical and experimental data are consistent despite a little deviation between the two. This is possibly due to the approximations (such as first-order approximation) made in the present theory, which does reveal the most dominant processes observed in the experiment. However, one may improve the theoretical model by including more details to further match the experimental data. For example, the use of slightly chirped pulses in the experiment, which may change

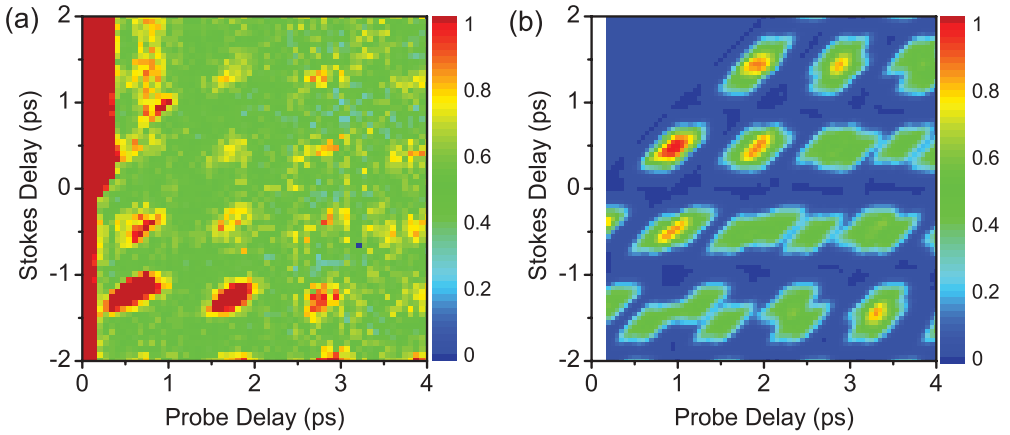

FIG. 8. (Color online) Two-dimensional FWM signal as a function of both the Stokes and probe delays. (a) Experimental measurements. (b) Theoretical results.

the distribution of the spots in the pattern, is not considered in the theoretical model.

V. CONCLUSION

We study the wave-packet dynamics in cesium dimers both experimentally and theoretically. In the experiment we use the coherent anti-Stokes Raman scattering spectroscopic technique. The temporal coherent control is achieved by arranging either the Stokes-pump-probe or pump-Stokes-probe timing sequences. The CARS signal exhibits different oscillations with specific periods determined by the wave packets' cycle motion induced either in the ground or excited states of Cs_2 molecules by varying the probe delay. Moreover, the CARS signal is also recorded by scanning both delays of the Stokes and probe pulses independently and the measured data display the two-dimensional periodic pattern.

An appropriate theoretical model based on the density matrix formalism is developed to explain the experimental results. The obtained approximate solutions enable us to reveal the physical mechanism for the complex processes that take place during the experiment. Depending on timing sequence of the input pulses we find out that at least four different types of coherent Raman scattering processes play crucial role in the overall wave-packet dynamics in cesium molecules. We perform the numerical simulations and show that the theoretical and experimental results are consistent.

The present coherent temporal control experimental technique can be used to create and manipulate the quantum interference between wave packets produced in different electronic states of cesium dimers whereas the present theory can presumably be extended to various molecules.

ACKNOWLEDGMENTS

The authors thank Marlan O. Scully for helpful discussions. This work was supported by the Office of Naval Research, the National Science Foundation (Grants No. PHY 354897 and No. 722800), the United States Air Force Office of Scientific Research under programs FA9550-10-1-0237 and FA9550-10-1-0561, the Texas Advanced Research Program (Grant No. 010366-0001-2007), the Army Research Office (Grant No. W911NF-07-1-0475), and the Robert A. Welch Foundation (Grant No. A1547).

APPENDIX A

For the first pathway in the Stokes-pump-probe pulse sequence in Fig. 2(a), the Stokes pulse first creates the coherence given by

$$\rho_{ab}(t) \simeq i\sqrt{\frac{\pi}{2}}\rho_{bb}^{(-\infty)}\wp_{ab}\mathcal{E}_s\sigma_s e^{-\frac{1}{2}[\sigma_s(\nu_s-\omega_{ab})]^2}e^{-i\omega_{ab}(t-\tau_s)} \times e^{i\mathbf{k}_s\cdot\mathbf{x}}\theta(t-\tau_s) \tag{A1}$$

under the first-order approximation. The pump pulse then interacts with the sample and induces the coherence given by

$$\rho_{a'a}(t) \simeq \frac{\pi}{2}\rho_{bb}^{(-\infty)}\wp_{a'b}\wp_{ba}\mathcal{E}_s\mathcal{E}_p\sigma_s\sigma_p e^{-\frac{1}{2}[\sigma_s(\nu_s-\omega_{ab})]^2} \times e^{-\frac{1}{2}[\sigma_p(\nu_p-\omega_{a'b})]^2} \times e^{i\omega_{ab}(\tau_p-\tau_s)}e^{-i\omega_{a'a}(t-\tau_p)} \times e^{i(\mathbf{k}_p-\mathbf{k}_s)\cdot\mathbf{x}}\theta(t-\tau_p). \tag{A2}$$

At last the probe pulse creates the coherence given by

$$\rho_{a'c}(t) \simeq -i\left(\frac{\pi}{2}\right)^{3/2}\rho_{bb}^{(-\infty)}\wp_{a'b}\wp_{ba}\wp_{ac}\mathcal{E}_s\mathcal{E}_p\mathcal{E}_{pr}\sigma_s\sigma_p\sigma_{pr}e^{-\frac{1}{2}[\sigma_s(\nu_s-\omega_{ab})]^2}e^{-\frac{1}{2}[\sigma_p(\nu_p-\omega_{a'b})]^2}e^{-\frac{1}{2}[\sigma_{pr}(\nu_{pr}-\omega_{ac})]^2} \times e^{i\omega_{ab}(\tau_p-\tau_s)}e^{-i\omega_{a'a}(\tau_{pr}-\tau_p)}e^{-i\omega_{a'c}(t-\tau_{pr})}e^{i(\mathbf{k}_p-\mathbf{k}_s+\mathbf{k}_{pr})\cdot\mathbf{x}}\theta(t-\tau_{pr}). \tag{A3}$$

Here, in the resulting coherence term, $\rho_{a'c}$, the phase-matching condition, $\mathbf{k}_{\text{Signal}} = \mathbf{k}_p - \mathbf{k}_s + \mathbf{k}_{pr}$ is satisfied. Before calculating the signal intensity, let us introduce the decay rate ($\gamma \sim 1\ \text{ns}^{-1}$) into the resulting coherence $\rho_{a'c}$ equation by hand and rewrite

Eq. (A3) as

$$\rho_{a'c}(t) \simeq -i\left(\frac{\pi}{2}\right)^{3/2} \rho_{bb}^{(-\infty)} \wp_{a'b}\wp_{ba}\wp_{ac}\mathcal{E}_s\mathcal{E}_p\mathcal{E}_{pr}\sigma_s\sigma_p\sigma_{pr} e^{-\frac{1}{2}[\sigma_s(\nu_s-\omega_{ab})]^2} e^{-\frac{1}{2}[\sigma_p(\nu_p-\omega_{a'b})]^2} e^{-\frac{1}{2}[\sigma_{pr}(\nu_{pr}-\omega_{ac})]^2}$$
$$\times e^{-i\omega_{a'}(\tau_{pr}-\tau_p)} e^{i\omega_a(\tau_{pr}-\tau_s)} e^{-i\omega_b(\tau_p-\tau_s)} e^{-\gamma(t-\tau_{pr})} e^{-i\omega_{a'c}(t-\tau_{pr})} e^{i(\mathbf{k}_p-\mathbf{k}_s+\mathbf{k}_{pr})\cdot\mathbf{x}}\theta(t-\tau_{pr}). \tag{A4}$$

Under the RWA approximation, we plug this result into Eq. (7) to find the signal intensity as

$$S \simeq \sum_{a',a_1'}\sum_{a,a_1}\sum_{b,b_1}\sum_{c,c_1}\left(\frac{\pi}{2}\right)^3 |\rho_{bb}^{(-\infty)}|^2 \wp_{ca'}\wp_{a'b}\wp_{ba}\wp_{ac}\wp_{a_1'c_1}\wp_{b_1a_1'}\wp_{a_1b_1}\wp_{c_1a_1}(\mathcal{E}_s\mathcal{E}_p\mathcal{E}_{pr}\sigma_s\sigma_p\sigma_{pr})^2$$
$$\times e^{-\frac{1}{2}[\sigma_s(\nu_s-\omega_{ab})]^2} e^{-\frac{1}{2}[\sigma_p(\nu_p-\omega_{a'b})]^2} e^{-\frac{1}{2}[\sigma_{pr}(\nu_{pr}-\omega_{ac})]^2} \times e^{-\frac{1}{2}[\sigma_s(\nu_s-\omega_{a_1b_1})]^2} e^{-\frac{1}{2}[\sigma_p(\nu_p-\omega_{a_1'b_1})]^2} e^{-\frac{1}{2}[\sigma_{pr}(\nu_{pr}-\omega_{a_1c_1})]^2}$$
$$\times e^{-i\omega_{a'a_1'}(\tau_{pr}-\tau_p)} e^{i\omega_{aa_1}(\tau_{pr}-\tau_s)} e^{-i\omega_{bb_1}(\tau_p-\tau_s)} \int_{\tau_{pr}}^{\infty} e^{-2\gamma(t-\tau_{pr})} e^{-i(\omega_{a'c}-\omega_{a_1'c_1})(t-\tau_{pr})} dt + \text{c.c.}. \tag{A5}$$

The integral in Eq. (A5) gives

$$\int_{\tau_{pr}}^{\infty} e^{-2\gamma(t-\tau_{pr})} e^{-i(\omega_{a'c}-\omega_{a_1'c_1})(t-\tau_{pr})} dt = \frac{1}{2\gamma + i\left(\omega_{a'c}-\omega_{a_1'c_1}\right)} \approx \begin{cases} \frac{1}{2\gamma} & \omega_{a'c} = \omega_{a_1'c_1} \\ \frac{1}{i\left(\omega_{a'c}-\omega_{a_1'c_1}\right)} & \omega_{a'c} \neq \omega_{a_1'c_1} \end{cases}. \tag{A6}$$

Under the underdamped condition, $2\gamma \ll |\omega_{a'c} - \omega_{a_1'c_1}|$. The contribution from the term $\frac{1}{2\gamma}$ is dominating, so it is reasonable to drop the small terms with $a' \neq a_1'$ or $c \neq c_1$, and the signal intensity reads as Eq. (8).

APPENDIX B

In this Appendix, we simplify Eq. (8) under some approximations. Since the pulse width is finite, it is reasonable to consider the first four main contributions from the near-resonant vibrational levels in Eq. (8). It gives

$$S \propto \sum_{a',a,b,c} \{\wp_{ca'}\wp_{a'b}\wp_{ba}\wp_{ac}\wp_{a'c}\wp_{ba'}\wp_{ab}\wp_{ca} + \wp_{ca'}\wp_{a'b}\wp_{ba}\wp_{ac}\wp_{a'c}\wp_{b+1,a'}\wp_{a,b+1}\wp_{ca}\cos[\omega_{b+1,b}(\tau_p-\tau_s)]$$
$$+ \wp_{ca'}\wp_{a'b}\wp_{ba}\wp_{ac}\wp_{a'c}\wp_{ba'}\wp_{a+1,b}\wp_{c,a+1}\cos[\omega_{a+1,a}(\tau_{pr}-\tau_s)]$$
$$+ \wp_{ca'}\wp_{a'b}\wp_{ba}\wp_{ac}\wp_{a'c}\wp_{b+1,a'}\wp_{a+1,b+1}\wp_{c,a+1}\cos[\omega_{a+1,a}(\tau_{pr}-\tau_s) - \omega_{b+1,b}(\tau_p-\tau_s)]\}. \tag{B1}$$

From Fig. 3(a), we notice that the pump and probe fields couple the (ν', ν'') transitions located on the upper lines, which are composed by dark red and dark blue dots, while the Stokes field couples the (ν', ν'') transition located on the lower lines composed by dark orange dots. After taking care of the sign of each integral in Fig. 3(a), we can make the following approximations for those large dipole moments in Eq. (B1):

$$\wp_{ab} \simeq \wp_{a+1,b} \simeq \wp_{a,b+1} \simeq \wp_{a+1,b+1}, \quad \wp_{ca} \simeq -\wp_{c,a+1}, \quad \wp_{ba'} \simeq -\wp_{b+1,a'}. \tag{B2}$$

Under these approximations, we obtain Eq. (10).

[1] *Femtochemistry and Femtobiology: Ultrafast Events in Molecular Science*, James T. Hynes (Elsevier, Amsterdam, 2004).

[2] M. Dantus and V. Lozovoy, Chem. Rev. **104**, 1813 (2004).

[3] A. H. Zewail, Science **242**, 1645 (1988).

[4] G. Rodriguez and J. G. Eden, Chem. Phys. Lett. **205**, 371 (1993).

[5] G. Rodriguez, P. C. John, and J. G. Eden, J. Chem. Phys. **103**, 10473 (1995).

[6] A. L. Oldenburg, P. C. John, and J. G. Eden, J. Chem. Phys. **113**, 11009 (2000).

[7] T. Siebert, M. Schmitt, A. Vierheilig, G. Flachenecker, V. Engel, A. Materny, and W. Kiefer, J. Raman Spectrosc. **31**, 25 (2000).

[8] A. Scaria, V. Namboodiri, J. Konradi, and A. Materny, J. Chem. Phys. **127**, 144305 (2007).

[9] J. Liebers, A. Scaria, A. Materny, and U. Kleinekathöfer, J. Raman Spectrosc. **40**, 822 (2009).

[10] T. Chen, V. Engel, M. Heid, W. Kiefer, G. Knopp, A. Materny, S. Meyer, R. Pausch, M. Schmitt, H. Schwoerer, and T. Siebert, J. Mol. Struct. **480**, 33 (1999); **481**, 33 (1999).

[11] D. Avisar and D. J. Tannor, Phys. Rev. Lett. **106**, 170405 (2011).

[12] D. Pestov, R. K. Murawski, G. O. Ariunbold, X. Wang, M. Zhi, A. V. Sokolov, V. A. Sautenkov, Y. V. Rostovtsev, A. Dogariu, Y. Huang, and M. O. Scully, Science **316**, 265 (2007).

[13] D. Pestov, X. Wang, G. O. Ariunbold, R. K. Murawski, V. A. Sautenkov, A. Dogariu, A. V. Sokolov, and M. O. Scully, Proc. Natl. Acad. Sci. USA **105**, 422 (2008).
[14] U. Banin, A. Bartana, S. Ruhman, and R. Kosloff, J. Chem. Phys. **101**, 8461 (1994).
[15] E. Gershgoren, J. Vala, R. Kosloff, and S. Ruhman, J. Phys. Chem. A **105**, 5081 (2001).
[16] Vadim V. Lozovoy, Bruna I. Grimberg, Igor Pastirk, and Marcos Dantus, Chem. Phys. **267**, 99 (2001).
[17] G. O. Ariunbold, V. A. Sautenkov, and M. O. Scully, J. Opt. Soc. Am. B **28**, 462 (2011).
[18] G. O. Ariunbold, V. A. Sautenkov, and M. O. Scully, Opt. Lett. **37**, 2400 (2012).
[19] H. Goto, H. Katsuki, H. Ibrahim, H. Chiba, and K. Ohmori, Nature Phys. **7**, 383 (2011).
[20] S. T. Roberts, J. J. Loparo, K. Ramasesha, and A. Tokmakoff, Opt. Commun. **284**, 1062 (2011).
[21] X. Dai, A. D. Bristow, D. Karaiskaj, and S. T. Cundiff, Phys. Rev. A **82**, 052503 (2010).
[22] M. E. Siemens, G. Moody, H. Li, A. D. Bristow, and S. T. Cundiff, Opt. Express **18**, 17699 (2010).
[23] J. Faeder, I. Pinkas, G. Knopp, Y. Prior, and D. J. Tannor, J. Chem. Phys. **115**, 8440 (2001).
[24] T. Siebert, M. Schmitt, S. Gräfe, and V. Engel, J. Raman Spectrosc. **37**, 397 (2006).
[25] J. P. Kuehner, S. V. Naik, W. D. Kulatilaka, N. Chai, N. M. Laurendeau, R. P. Lucht, M. O. Scully, S. Roy, A. K. Patnaik, and J. R. Gord, J. Chem. Phys. **128**, 174308 (2008).
[26] M. O. Scully and M. S. Zubairy, *Quantum Optics* (Cambridge University Press, Cambridge, 1997).
[27] R. K. Murawski, Y. V. Rostovtsev, Z.-E. Sariyanni, V. A. Sautenkov, S. Backus, D. Raymondson, H. C. Kapteyn, M. M. Murnane, and M. O. Scully, Phys. Rev. A **77**, 023403 (2008).
[28] L. Yuan, G. O. Ariunbold, R. K. Murawski, D. Pestov, X. Wang, A. K. Patnaik, V. A. Sautenkov, A. V. Sokolov, Y. V. Rostovtsev, and M. O. Scully, Phys. Rev. A **81**, 053405 (2010).
[29] P. Atkins and R. Friedman, *Molecular Quantum Mechanics*, 4th ed. (Oxford University Press, New York, 2005).
[30] B. W. Xu, J. M. Gunn, J. M. Dela Cruz, V. V. Lozovoy, and M. Dantus, J. Opt. Soc. Am. B **23**, 750 (2006).
[31] A. N. Nesmeyanov, *Vapor Pressure of the Chemical Elements*, edited by G. Robert (Elsevier, Amsterdam, 1963).
[32] D. Steele and E. R. Lippincott, Rev. Mod. Phys. **34**, 239 (1962).
[33] G. Herzberg, *Molecular Spectra and Molecular Structure, I. Spectra of Diatomic Molecules*, 2nd ed. (D. Van Nostrand, New York, 1950).